

Anisotropic nematic fluctuations above the ferroquadrupolar transition in TmVO_4

Z. Wang,¹ I. Vinograd,¹ Z. Mei,¹ P. Menegasso,² D. Garcia,¹ P. Massat,³ I. R. Fisher,³ and N. J. Curro¹

¹*Department of Physics, University of California, Davis, California 95616, USA*

²*Instituto de Física “Gleb Wataghin”, UNICAMP, Campinas-SP, 13083-859, Brazil*

³*Geballe Laboratory for Advanced Materials and Department of Applied Physics, Stanford University, CA 94305, USA*

(Dated: August 25, 2021)

TmVO_4 exhibits ferroquadrupolar order below 2.15 K with a well-isolated non-Kramers ground state doublet, and is a model system to understand Ising nematic order. We present ^{51}V nuclear magnetic resonance data as a function of field orientation in a single crystal. Although the spectra are well understood in terms of direct dipolar hyperfine couplings, the spin lattice relaxation rate exhibits strong anisotropy that cannot be understood in terms of magnetic fluctuations. We find that the spin lattice relaxation rate scales with the shear elastic constant associated with the ferroquadrupole phase transition, suggesting that quadrupole (nematic) fluctuations dominate the spin lattice relaxation for in-plane fields.

I. INTRODUCTION

Recently there has been growing interest in the behavior of electronic Ising nematicity, which may play a role in the low temperature behavior of a number of strongly correlated electron systems. The phase diagram of the iron-based superconductors is dominated by C_4 symmetry breaking of the spin and orbital degrees of freedom, accompanied by a tetragonal-to-orthorhombic structural transition [1]. The physical origin of the nematicity is yet to be established, and might even be different in different families of compounds, with possible contributions both from orbital effects and spin fluctuations. The correlation between large values of the nematic susceptibility, a putative nematic quantum critical point, and optimal superconductivity in several materials, point to a possible role for nematic fluctuations in the pairing interaction, as well as non-Fermi-liquid behavior in the normal state [2–5]. Electronic nematic correlations are also present in the high temperature superconducting cuprates [6, 7]. Disentangling the effects of nematicity can be complicated by the presence of other intertwined order parameters in such systems. It is challenging to discern whether nematic or antiferromagnetic fluctuations dominate, especially in a conducting system [8]. Moreover, strain couples to the nematic order, hence quenched random disorder around dopants may give rise to inhomogeneous glassy behavior [9, 10]. It is therefore important to investigate critical fluctuations in an Ising nematic system in the absence of metallicity or inhomogeneous strain fields.

Ferroquadrupolar ordering of non-Kramers doublets in 4f materials offers an important avenue to investigate Ising nematicity [11]. Specifically, ferroquadrupole order breaks all the same symmetries as Ising nematic order (and hence is a specific realization of nematic order), with the advantage that the underlying effective Hamiltonian describing the low-temperature behavior is well-understood. TmVO_4 is an insulator with Tm ions in the $4f^{12}$ configuration ($L = 5$, $S = 1$, $J = 6$) that crystallizes in space group $I41/amd$ (see inset of Fig. 1). The tetragonal crystal field splits the $J = 6$ multiplet giving rise to a

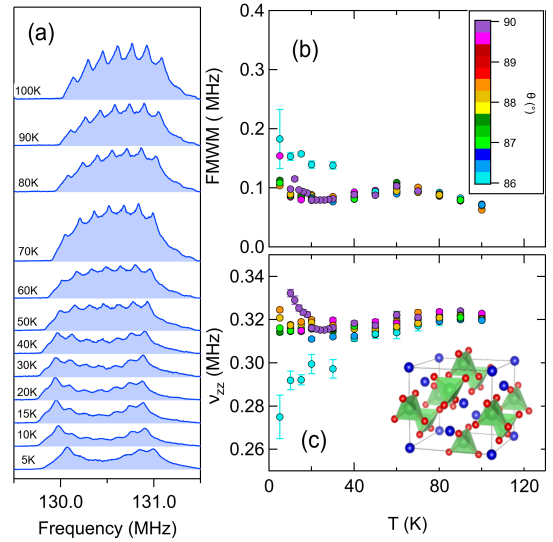


FIG. 1. (a) ^{51}V spectra in TmVO_4 at 11.7294 T for $\mathbf{H}_0 \perp c$ at several different temperatures. The full-width half maximum (b) and quadrupolar splitting (c) versus temperature for several different angles, θ . The inset shows the unit cell structure. Tm is blue, V is green (within the pyramids) and O is red.

Γ_5 ground state doublet separated by a gap of ~ 77 K to the lowest excited state [12, 13]. The wavefunctions of the ground state doublet are $|\psi_{1,2}\rangle = e|\pm 5\rangle + f|\pm 1\rangle + g|\mp 3\rangle$ in the J_z basis, where $e \approx 0.92$, $f \approx -0.37$, and $g \approx 0.12$. The degeneracy of these ground states cannot be lifted by a magnetic field perpendicular to the z -direction because $\langle \psi_{1,2} | J_{\pm} | \psi_{1,2} \rangle = 0$, hence these form a non-Kramers doublet. The doublet can, however, be linearly split by either a magnetic field oriented along the c -axis, or by lattice strains with either a B_{1g} ($x^2 - y^2$) or B_{2g} (xy) symmetry. Quadrupole-quadrupole interactions mediated by the lattice dominate the magnetic interactions, and the material undergoes a cooperative Jahn-Teller ferroquadrupolar ordering with a B_{2g} symmetry at $T_Q = 2.15\text{K}$, accompa-

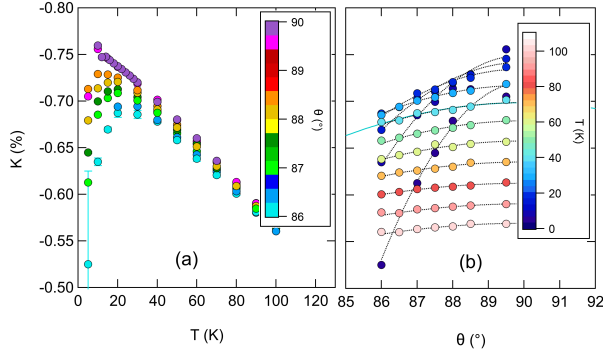


FIG. 2. magnetic shift, K , versus temperature (a) and versus angle (b). The dotted lines are fits as described in the text.

nied by an orthorhombic lattice distortion of the same symmetry [14]. The low-temperature behavior of the Tm quadrupoles can be well-described by the transverse field Ising model, in which pseudospins ($\tilde{S} = 1/2$) experience in-plane ferroquadrupolar Ising couplings and couple to a transverse magnetic field along the z -axis [11]. These fields will enhance the fluctuations of the pseudospins and can tune the system to an Ising-nematic quantum phase transition. This material thus offers an important platform to investigate quantum critical nematic fluctuations in an insulator.

In order to better understand the nature of these fluctuations we have investigated ^{51}V ($I = 7/2$, $Q = 52$ mb, 99.75% abundant) NMR in a single crystal of TmVO_4 in a magnetic field $\mathbf{H}_0 = 11.72$ T oriented perpendicular to the c -axis. We find that the magnetic shift and spin-lattice-relaxation rate are strongly angular dependent (rotating the field in the $a-c$ plane) below ~ 80 K, reflecting the anisotropy of the ground state doublet. The spin-lattice-relaxation rate is non-monotonic, exhibiting a large enhancement at low temperature that may be associated with critical nematic fluctuations. The spectrum exhibits a strong temperature-dependent magnetic broadening at low temperatures caused by inhomogeneous magnetic demagnetization fields.

II. NMR SPECTRA AND MAGNETIC SHIFT

TmVO_4 crystals were grown from a $\text{Pb}_2\text{V}_2\text{O}_7$ flux using 4 mole percent of Tm_2O_3 , following the methods described in [15, 16]. The crystals have a rod-like morphology with the c -axis along the long axis. A single crystal of approximate dimension $1\text{mm} \times 1\text{mm} \times 4\text{mm}$ was selected and mounted on a cryogenic goniometer NMR probe. The magnetic susceptibility is strongly anisotropic, reflecting that of the unusual g -factor ($g_c = 10.2$, $g_\perp \approx 0$) of the ground state doublet. Although a crystal mounted with $c \perp \mathbf{H}_0$ experiences zero torque, it is an unstable equilibrium and there is a large torque for infinitesimal deviations from 90° . To al-

leviate this issue we secured the crystal with epoxy to a mounting plate that itself is rotated. Spin echoes were acquired at several different frequencies, and the Fourier transforms were summed to measure the full spectra including all nuclear spin transitions. Fig. 1(a) shows several representative spectra of the ^{51}V as a function of temperature. There are seven peaks separated by the quadrupolar interaction. Because the V has axial symmetry, the peaks frequencies are given by:

$$\nu = \gamma H_0 (1 + K(\theta)) + n\nu_q(\theta), \quad (1)$$

where the magnetic, $K(\theta)$, and quadrupolar, $\nu_q(\theta)$, shifts vary with the angle θ between the c -axis and \mathbf{H}_0 :

$$K(\theta) = K_{cc} \cos^2 \theta + K_{aa} \sin^2 \theta \quad (2)$$

$$\nu_q(\theta) = \nu_{zz} (3 \cos^2 \theta - 1) / 2. \quad (3)$$

Here $\gamma = 11.193$ MHz/T, $n = -3, \dots, 3$, $\nu_{zz} = eQV_{zz}/12h$ and V_{zz} is the electric field gradient at the V site. We measured the spectra for several angles $86^\circ \leq \theta \leq 90^\circ$ and fit the spectra to a sum of Lorentzians. The temperature and angular dependence of the linewidths, EFG, and magnetic shifts are shown in Figs. 1(b, c) and 2(a).

We find that the EFG is similar to previous measurements, [12, 17] however the spectra are broad. For this orientation, the quadrupolar splitting is $\nu_{zz}/2$, which is comparable to the FWHM of each resonance. As a result, the individual peaks become difficult to resolve at low temperatures. Each of the satellite resonances has the same linewidth, implying that the broadening is due to magnetic field inhomogeneity within the sample. Moreover, we find that the spectra are narrower at lower applied fields and that the FWHM varies approximately linearly with field. Since the susceptibility is strongly anisotropic, distortions of the internal field \mathbf{B} due to demagnetization effects within the needle-like prism of the crystal can create a large distribution of local resonance frequencies [18]. The spectra also display a suppression of intensity for the inner satellites, particularly at low temperature. This phenomenon arises due to fast spin-spin decoherence rates (T_2^{-1}) with high spin nuclei [19].

The magnetic shift shown in Fig. 2 is negative and strongly angular dependent at low temperature. We fit the angular dependence to extract the tensor components K_{aa} and K_{cc} , shown as dotted lines in Fig. 2(b). This approach enables us to extract the magnetic shift for the c direction without needing to fully align the crystal in this orientation, albeit the error bars for K_{cc} are larger than for K_{aa} . The temperature dependence of K_{aa} and K_{cc} are shown in Fig. 3(a). K_{cc} is large and positive. Fig. 3(b) shows these shift components plotted versus the bulk susceptibility $\chi_{aa,cc}$, which was measured independently in a SQUID magnetometer. The shift varies linearly with susceptibility as $K_{\alpha\alpha} = K_{\alpha\alpha}^{orb} + A_{\alpha\alpha}\chi_{\alpha\alpha}$, where $A_{\alpha\beta}$ are the components of the hyperfine coupling tensor. We find that $K_{aa}^{orb} = -0.315 \pm 0.009\%$, $K_{cc}^{orb} = -0.4 \pm 0.1\%$, $A_{aa} = -0.32 \pm 0.07$ kOe/ μ_B and $A_{cc} = 1.29 \pm 0.05$ kOe/ μ_B .

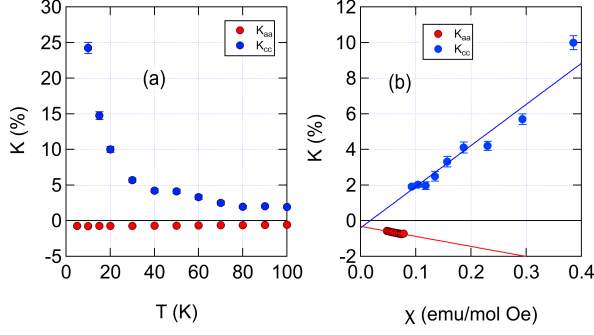


FIG. 3. K_{aa} and K_{cc} versus temperature (a) and versus bulk susceptibility (b). The solid lines are fits as described in the text.

These values of the hyperfine couplings are consistent with a direct dipolar coupling mechanism between the Tm moments and the V nuclear spins. The direct dipolar coupling is given by: $A_{\alpha\beta}^{dip} = \sum_i (\nabla \times \mathbf{A}_i)_\alpha / \mu_\beta$, where $\mathbf{A}_i = \mu \times \mathbf{r}_i / r_i^3$ is the vector potential of a dipole moment, μ , located at lattice site \mathbf{r}_i relative to a central nucleus. For the TmVO₄ lattice, we estimate $A_{aa}^{dip} = A_{bb}^{dip} = -0.336$ kOe/ μ_B and $A_{cc}^{dip} = 0.671$ kOe/ μ_B at the V site. The theoretical value for the perpendicular direction is the same as the measured value within the error limits. For the c axis, the theoretical value is within a factor of two of the measured values, and it is likely there are larger systematic measurement errors involved in extracting this value. Thus the anisotropic magnetic shift tensor can be fully explained via direct dipolar interactions, as expected for an insulator.

III. SPIN LATTICE RELAXATION RATE

The spin-lattice-relaxation rate, T_1^{-1} , was measured by applying inversion pulses at the central transition ($n = 0$) and measuring the echo intensity as a function of recovery time. The magnetization recovery was fit to the standard expression for magnetic fluctuations: $M(t) = M_0 (1 - 2f\phi(t/T_1))$, where M_0 is the equilibrium magnetization, f is the inversion fraction, and

$$\phi(t) = \frac{1225}{1716}e^{-28t} + \frac{75}{364}e^{-15t} + \frac{3}{44}e^{-6t} + \frac{1}{84}e^{-t}. \quad (4)$$

This expression fits the data well without the need for a stretching exponent. Fig. 4 shows the temperature and angular dependence of T_1^{-1} . For $\theta = 90^\circ$, T_1^{-1} decreases strongly below 80 K as the excited crystal field levels are thermally depopulated. In this temperature range T_1^{-1} become strongly angular dependent, increasing by more than a factor of 30 as the field \mathbf{H}_0 rotates by only 4° away from the perpendicular configuration. This behavior likely reflects the anisotropy of the g factor of the ground state doublet, however the anisotropy of T_1^{-1} is

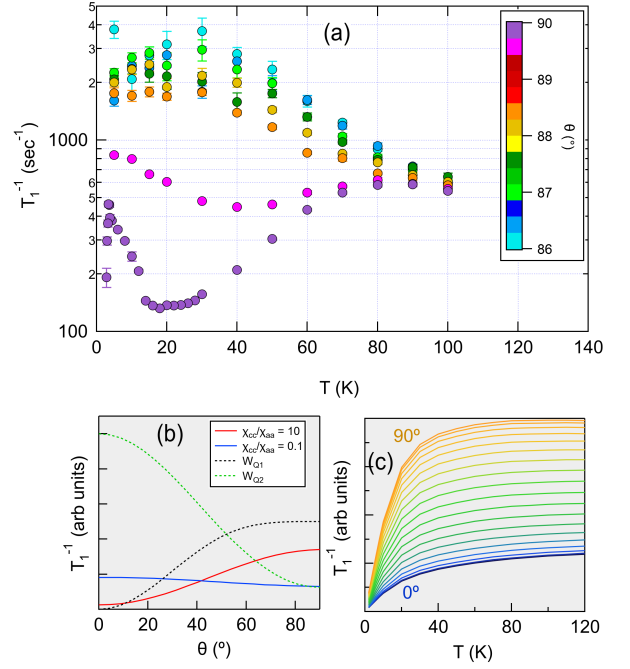


FIG. 4. (a) T_1^{-1} vs temperature for multiple angles. (b) Calculated T_1^{-1} versus θ for magnetic fluctuations (solid lines) and for quadrupole fluctuations (dashed lines). (c) Calculated T_1^{-1} versus temperature and angle using Eq. 5, where the angle is increased in 5° increments between 0 and 90° .

puzzling. If the relaxation is driven by magnetic fluctuations of the Tm ground state, then T_1^{-1} should exhibit a *maximum* at $\theta = 90^\circ$ rather than a minimum because fluctuations of the non-Kramers doublet should lie exclusively along the c -axis. Therefore $T_1^{-1}(0^\circ)$ should be much smaller than $T_1^{-1}(90^\circ)$, in contrast to our observations.

A. Magnetic fluctuations

On the other hand, the hyperfine couplings can give rise to a more complicated relationship between the direction of the Tm moments and the direction of the hyperfine fields. To properly account for these couplings we use the Moriya expression:

$$T_{1m}^{-1} = \gamma^2 k_B T \lim_{\omega \rightarrow 0} \sum_{\mathbf{q}, \alpha, \beta} \mathcal{F}_{\alpha\beta}(\mathbf{q}) \frac{\text{Im} \chi_{\alpha\beta}(\mathbf{q}, \omega)}{\hbar \omega}, \quad (5)$$

where the form factors $\mathcal{F}_{\alpha\beta}(\mathbf{q})$ (see Appendix A for details) depend on the local dipolar hyperfine couplings, and $\chi_{\alpha\beta}(\mathbf{q}, \omega)$ is the dynamical magnetic susceptibility of the Tm moments. For simplicity we only include the two nearest neighbor and four next-nearest neighbor Tm atoms in the form factors. Because the Tm system exhibits ferroquadrupolar order at T_Q , we assume that the structure of the dynamical susceptibility can be modeled

as:

$$\chi_{\alpha\alpha}(\mathbf{q}, \omega) = \frac{\chi_{\alpha\alpha}(T)}{\xi^{-2} + f(\mathbf{q}) - i\omega/\Gamma q} \quad (6)$$

where ξ is a correlation length, Γ is a characteristic fluctuation energy, $f(\mathbf{q}) = q_x^2 + q_y^2 + \eta q_z^2$, η is a dimensionless parameter that reflects the tetragonal nature, and $\chi_{\alpha\alpha}(T)$ is the static ($\mathbf{q} = 0$) susceptibility. ξ and η are unknown parameters, but we compute the temperature and angular dependence using $\xi = 2$ and $\eta = 1/2$. Fig. 4(b) shows the expected angular dependence of T_{1m}^{-1} for $\chi_{cc}/\chi_{aa} = 10$ (red), close to the experimental value, and for $\chi_{cc}/\chi_{aa} = 0.1$ (blue). The former clearly exhibits a maximum of T_{1m}^{-1} at $\theta = 90^\circ$, in contrast to our observations. The latter exhibits a shallow minimum at 90° , but the susceptibility anisotropy does not agree with experiment. Fig. 4(c) shows the temperature dependence using the measured values of the static susceptibility. Although there is an overall decrease in T_{1m}^{-1} at lower temperatures, the detailed temperature dependence does not match experiment, and the calculated T_1^{-1} still exhibits a maximum for $\theta = 90^\circ$ at all temperatures. Despite the complex form factors for the direct dipolar couplings, the expected magnetic fluctuations of the Tm ground state cannot explain the observed increase in T_1^{-1} as the field rotates out of the plane.

B. Quadrupolar fluctuations

An alternative explanation is that the spin-lattice-relaxation rate is dominated by quadrupolar fluctuations rather than magnetic. The Tm quadrupole moments couple to the EFG at the V site, giving rise to a second nuclear quadrupolar relaxation channel [8]. The enhancement of T_1^{-1} below 20K for $\theta = 90^\circ$ may represent the growth of critical fluctuations near T_Q . Note that changing θ by only 0.25° dramatically alters T_1^{-1} , which is close to the limit of precision of our goniometer. Thus it is possible that the enhancement below 20K may vanish or become smaller for better alignment. In the presence of both magnetic and quadrupolar relaxation, the expression for $\phi(t)$ (Eq. 4) changes, and includes three independent rates: T_{1m}^{-1} , W_{Q1} and W_{Q2} , where the latter two are associated with $\Delta m = \pm 1$ and $\Delta m = \pm 2$ quadrupolar relaxation. We are unable, however, to independently extract these parameters with sufficient resolution. Moreover, the line broadening observed in Fig. 1 also means that the magnetization relaxation at the central transition may also include contributions from nearby satellite transitions, further complicating any attempts to extract the independent relaxation channels. Nevertheless, it is instructive to consider the case where quadrupole fluctuations dominate and magnetic fluctuations can be neglected.

Quadrupolar relaxation is driven by fluctuations of the spherical tensor components of the EFG: $V_{\pm 1} = V_{zx} \pm iV_{zy}$ and $V_{\pm 2} = \frac{1}{2}(V_{xx} - V_{yy}) \pm iV_{xy}$, where the $V_{\alpha\beta}$ are

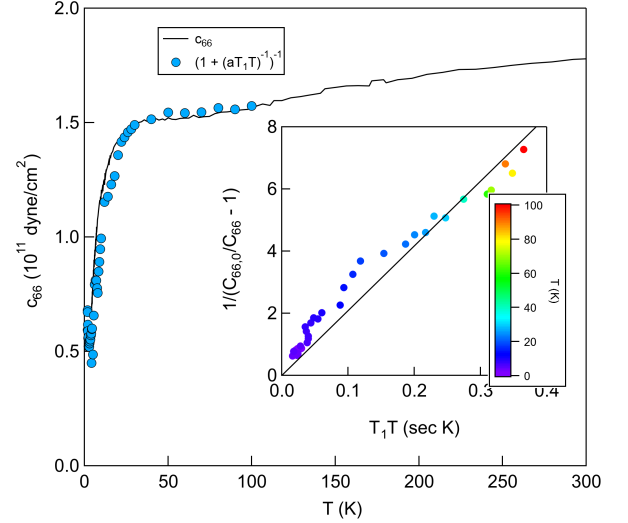


FIG. 5. The shear elastic stiffness coefficient c_{66} (solid line, reproduced from [21]) and the quantity $1/(1 + (aT_1T)^{-1})$ as a function of temperature. INSET: $1/(c_{66,0}/c_{66} - 1)$ versus T_1T , with temperature implicit. The solid black line is the best linear fit, giving $a = 18.5 \pm 0.4 \text{ sec}^{-1} \text{ K}^{-1}$.

the EFG tensor components relative to the direction of \mathbf{H}_0 . These give rise to nuclear spin relaxation rates:

$$W_{Q1,Q2} = (eQ/\hbar)^2 \int_0^\infty \langle V_{+1,2}(\tau) V_{-1,2}(0) \rangle e^{-\omega_L \tau} d\tau \quad (7)$$

where ω_L is the Larmor frequency [20]. The nematic order in this system has B_{2g} symmetry, so $V_{xx} - V_{yy} \neq 0$, where z corresponds to the c -direction and x and y are along the principal axes of the EFG tensor, which are rotated 45° relative to the tetragonal a -axes. Above T_Q fluctuations of $V_{\pm 2}$ should dominate those of $V_{\pm 1}$, and as a result we anticipate that $W_{Q1}(\theta = 0)$ can be neglected. As the field is rotated towards the plane, the EFG tensor components change, and the relaxation rates become angular dependent (see Appendix B for details):

$$W_{Q2}(\theta)/W_{Q2}(0) = (\cos^4 \theta + 6 \cos^2 \theta + 1) / 8 \quad (8)$$

$$W_{Q1}(\theta)/W_{Q2}(0) = \sin^2 \theta (\cos(2\theta) + 3) / 4. \quad (9)$$

These quantities are shown in Fig. 4(b) as dashed lines. W_{Q2} exhibits a minimum for $\theta = 90^\circ$, whereas W_{Q1} is nearly independent of θ at this angle. This behavior agrees qualitatively with our observations, but the increases we observe are in fact a much stronger function of angle than expected for quadrupolar relaxation. Rotating θ by 1 - 2° out of the plane enhances T_1^{-1} by an order of magnitude, whereas W_{Q2} exhibits only a quadratic minimum at this angle.

The interpretation that relaxation is driven by quadrupole fluctuations is supported by comparisons of the temperature dependence of T_1^{-1} with that of the shear elastic stiffness coefficient, c_{66} , which softens with

decreasing temperature and vanishes at T_Q [21]. This behavior is driven by the nematic susceptibility: $\chi_{nem} = c_{66,0}(1 - c_{66,0}/c_{66})/\lambda^2$, where λ is the coupling between the lattice and the Tm 4f orbitals, and $c_{66,0}$ is the stiffness coefficient in the absence of the coupling [22]. If T_1^{-1} is also determined by the Tm orbital fluctuations, then $(T_1 T)^{-1} \sim \chi_{nem}$ (see Appendix C for details) [8, 23, 24]. We thus expect $T_1 T \sim (c_{66,0}/c_{66} - 1)^{-1}$, which is demonstrated in Fig. 5. The main panel compares the temperature dependence of c_{66} with the measured T_1^{-1} values, and the inset shows the scaling between the shear modulus and T_1^{-1} with temperature as an implicit parameter. The scaling evident in Fig. 5 suggests that the spin lattice relaxation is driven primarily by quadrupole fluctuations, which are reflected in the softening of c_{66} .

IV. DISCUSSION

A slightly different scaling relationship was found in the iron pnictide superconductors via a microscopic model that assumes that the nematicity arises in the magnetic susceptibility, which in turn affects the nuclei through a magnetic hyperfine interaction [22]. In TmVO₄, the nematicity arises from the Tm electronic orbitals, and the coupling to the nuclei may be through the quadrupolar interaction. Moreover, the pnictide model assumed the presence of Landau damping by a Fermi surface of quasiparticles, which is not the case for insulating TmVO₄. The relaxation in TmVO₄ must also involve a damping term, but the origin of this term is unknown. The fact that the scaling relationship in Fig. 4 holds suggests that this damping term is temperature independent.

Rotating the field away from 90° can enhance quadrupole fluctuations. A rotation of \mathbf{H}_0 by 4° corresponds to a field of 0.82 T along the c -axis. This is greater than the critical field of $H_c = 0.52$ T to suppress the long-range nematic order, which naturally enhances fluctuations of both $V_{\pm 2}$ and $V_{\pm 1}$. However, these critical fluctuations are not likely to persist to higher temperatures beyond $\sim 10T_Q$, thus are unlikely to be responsible for the large anisotropy observed up to 80K. An alternative scenario is that the higher CEF levels cannot be ignored. Indeed, even though the in-plane g -factor of the non-Kramers doublet vanishes in zero applied field, the excited CEF levels can be mixed into the ground state wavefunctions by an in-plane field. As a result, there can be an induced magnetic moment in the plane, which may also contribute to the relaxation [21].

It is likely that the spin lattice relaxation is dominated by both magnetic and quadrupolar fluctuations, however it is difficult to disentangle these two relaxation channels without more detailed measurements of the relaxation at the higher satellite transitions [20]. However, as illustrated in Fig. 1, the satellites are magnetically broadened and cannot be well resolved, especially at lower temperatures. This broadening is due to the demagnetization

field inhomogeneity of our crystal. In principle, it is possible to improve the spectral resolution by removing the sharp edges and corners of the sample and/or operating at lower applied fields, in order to better discern the individual satellite transitions.

Nuclear spin lattice relaxation rates have also been studied in both PrAlO₃ and CsCuCl₃, materials that exhibit structural distortions due to the cooperative Jahn-Teller effect with non-magnetic ground states [25–27]. In contrast to our observations in TmVO₄, T_1^{-1} did not exhibit any enhancement above the phase transition in these cases, even though the EFG changed below. On the other hand, unlike TmVO₄, the phase transitions in these cases are first order, thus T_1^{-1} should not reflect any critical slowing down. The spin-lattice-relaxation rate in the disordered state was analyzed in terms of magnetic (hyperfine) fluctuations, although the nuclei in question (²⁷Al, $I = 5/2$ and ¹³³Cs, $I = 7/2$) are quadrupolar and should be sensitive to fluctuations of the EFG.

In summary, we have measured the spectra and relaxation rates in TmVO₄ as a function of field direction oriented perpendicular to the c -axis. We find that the magnetic shift tensor agrees quantitatively with direct dipolar coupling between the V nuclear moments and the Tm 4f moments. The spin lattice relaxation rate exhibits a steep minimum for field oriented 90° to the c axis, which is inconsistent with purely magnetic fluctuations. We find that T_1 scales with the lattice constant for shear strain, c_{66} , which softens and vanishes at the nematic transition. It is likely that both quadrupolar and magnetic fluctuations are present and drive spin lattice relaxation. However, the origin of the steep angular dependence of T_1^{-1} remains an open question.

V. ACKNOWLEDGMENTS

We acknowledge helpful discussions with R. Fernandes. Work at UC Davis was supported by the NSF under Grants No. DMR-1807889 and PHY-1852581, as well as the UC Davis Seed Grant program. Crystal growth performed at Stanford University was supported by the Air Force Office of Scientific Research under award number FA9550-20-1-0252. P. M. was partially supported by the Gordon and Betty Moore Foundation Emergent Phenomena in Quantum Systems Initiative through Grant GBMF9068.

Appendix A: Magnetic Relaxation Form Factors

We assume that the dominant hyperfine fields at the V site arise from the two nearest neighbor and four next-nearest Tm moments, whose positions are given in Table I. We define:

$$\mathcal{A}_{\alpha\beta}(\mathbf{q}) = \sum_i e^{i\mathbf{q}\cdot\mathbf{r}_i} A_{\alpha\beta}^{dip} \quad (\text{A1})$$

where $A_{\alpha\beta}^{dip}$ is defined in the main text. For an applied field \mathbf{H}_0 oriented at angles θ and ϕ relative to the crystalline axes, the form factors are [28]:

$$\mathcal{F}_{\alpha\beta}(\mathbf{q}) = \sum_{\epsilon,\delta} [R_{x\epsilon}R_{x\delta} + R_{y\epsilon}R_{y\delta}] \mathcal{A}_{\epsilon\alpha}(\mathbf{q})\mathcal{A}_{\delta\beta}(-\mathbf{q}), \quad (\text{A2})$$

$$\mathbb{R} = \begin{pmatrix} \cos\theta \cos^2\phi + \sin^2\phi & \cos\theta \cos\phi \sin\phi - \cos\phi \sin\phi & \cos\phi \sin\theta \\ \cos\theta \cos\phi \sin\phi - \cos\phi \sin\phi & \cos^2\phi + \cos\theta \sin^2\phi & \sin\theta \sin\phi \\ -\cos\phi \sin\theta & -\sin\theta \sin\phi & \cos\theta \end{pmatrix}. \quad (\text{A3})$$

TABLE I. Position vectors for six nearest neighbor Tm sites to V, in spherical coordinates.

\mathbf{r}_i	r (Å)	θ (°)	ϕ (°)
1	3.13030	0	0
2	3.13030	180	0
3	3.86654	66.1218	0
4	3.86654	113.8782	90
5	3.86654	66.1218	180
6	3.86654	113.8782	270

Appendix B: Quadrupolar Relaxation Anisotropy

Equation 7 gives the expression for quadrupolar relaxation in terms of the spherical tensor components of the

$$\langle V_m'(\tau)V_{-m}'(0) \rangle = \sum_{m',m''} D_{2m'}^{(2)}(\phi,\theta) D_{-2m''}^{(2)}(\phi,\theta) \langle V_{m'}(\tau)V_{m''}(0) \rangle. \quad (\text{B3})$$

We assume that $\langle V_m(\tau)V_{m'}(0) \rangle = 0$ for all m, m' except for $m = -m' = 2$ and $m = m' = 1$. Moreover, we assume that $\langle V_2(\tau)V_{-2}(0) \rangle \gg \langle V_1(\tau)V_{-1}(0) \rangle$, since $\langle V_{\pm 2} \rangle \neq 0$ and $\langle V_{\pm 1} \rangle = 0$ in the nematic phase. We thus expect $W_{Q1}(\theta = 0) \approx 0$, and:

$$W_{Q2}(\theta)/W_{Q2}(0) = (\cos^4\theta + 6\cos^2\theta + 1)/8 \quad (\text{B4})$$

$$W_{Q1}(\theta)/W_{Q2}(0) = \sin^2\theta(\cos(2\theta) + 3)/4. \quad (\text{B5})$$

as given in the main text in Eqs. 8 and Eqs. 9.

where the $R_{\alpha\beta}$ are elements of the 3D rotation matrix:

EFG tensor. The quadrupolar interaction is only on-site, so there are no form factors. However, the EFG tensor must be rotated properly as the field direction changes. Under a rotation the tensor operators $V_m(\tau)$ transform as:

$$V_m'(\tau) = \sum_{m'} D_{mm'}^{(2)} V_{m'}(\tau) \quad (\text{B1})$$

where

$$D_{mm'}^{(l)}(\alpha, \beta, \gamma) = e^{-im\alpha} d_{mm'}^{(l)}(\beta) e^{-im'\gamma}, \quad (\text{B2})$$

are the Wigner D matrices, and the Euler angles are $(\alpha = \phi, \beta = \theta, \gamma = 0)$. The correlation functions $\langle V_m(\tau)V_{-m}(0) \rangle$ are thus given by:

Appendix C: Relaxation driven by nematic fluctuations

We note that Eq. 7 can be expressed in terms of the dynamical nematic susceptibility [8]:

$$W_{Q2}(0) = \left(\frac{eQ}{\hbar}\right)^2 k_B T \lim_{\omega \rightarrow 0} \sum_{\mathbf{q}} \frac{\text{Im}\chi_{nem}(\mathbf{q}, \omega)}{\hbar\omega}. \quad (\text{C1})$$

The dynamical susceptibility can be expressed phenomenologically as: $\chi_{nem}(\mathbf{q}, \omega) = \chi_{nem}(1 - i\omega/\omega_n)^{-1}$, where χ_{nem} is the static nematic susceptibility and ω_n is a damping term [23, 24]. In this case $W_{Q2}(0) = (eQ)^2 k_B T \chi_{nem}/\hbar^2 \omega_n$.

[1] R. M. Fernandes, A. V. Chubukov, and J. Schmalian, What drives nematic order in iron-based superconductors?, *Nat. Phys.* **10**, 97 (2014).

tors?, *Nat. Phys.* **10**, 97 (2014).

- [2] J.-H. Chu, H.-H. Kuo, J. G. Analytis, and I. R. Fisher, Divergent nematic susceptibility in an iron arsenide superconductor, *Science* **337**, 710 (2012).
- [3] H.-H. Kuo, J.-H. Chu, J. C. Palmstrom, S. A. Kivelson, and I. R. Fisher, Ubiquitous signatures of nematic quantum criticality in optimally doped Fe-based superconductors, *Science* **352**, 958 (2016).
- [4] S. Lederer, Y. Schattner, E. Berg, and S. A. Kivelson, Enhancement of superconductivity near a nematic quantum critical point, *Phys. Rev. Lett.* **114**, 097001 (2015).
- [5] T. A. Maier and D. J. Scalapino, Pairing interaction near a nematic quantum critical point of a three-band CuO_2 model, *Phys. Rev. B* **90**, 174510 (2014).
- [6] S. A. Kivelson, E. Fradkin, and V. J. Emery, Electronic liquid-crystal phases of a doped Mott insulator, *Nature* **393**, 550 (1998).
- [7] M. Vojta, Lattice symmetry breaking in cuprate superconductors: stripes, nematics, and superconductivity, *Advances in Physics* **58**, 699 (2009).
- [8] A. P. Dioguardi, T. Kissikov, C. H. Lin, K. R. Shirer, M. M. Lawson, H.-J. Grafe, J.-H. Chu, I. R. Fisher, R. M. Fernandes, and N. J. Curro, NMR evidence for inhomogeneous nematic fluctuations in $\text{BaFe}_2(\text{As}_{1-x}\text{P}_x)_2$, *Phys. Rev. Lett.* **116**, 107202 (2016).
- [9] A. P. Dioguardi, M. M. Lawson, B. T. Bush, J. Crocker, K. R. Shirer, D. M. Nisson, T. Kissikov, S. Ran, S. L. Bud'ko, P. C. Canfield, S. Yuan, P. L. Kuhns, A. P. Reyes, H.-J. Grafe, and N. J. Curro, NMR evidence for inhomogeneous glassy behavior driven by nematic fluctuations in iron arsenide superconductors, *Phys. Rev. B* **92**, 165116 (2015).
- [10] E. W. Carlson, K. A. Dahmen, E. Fradkin, and S. A. Kivelson, Hysteresis and noise from electronic nematicity in high-temperature superconductors, *Phys. Rev. Lett.* **96**, 097003 (2006).
- [11] A. V. Maharaj, E. W. Rosenberg, A. T. Hristov, E. Berg, R. M. Fernandes, I. R. Fisher, and S. A. Kivelson, Transverse fields to tune an Ising-nematic quantum phase transition, *Proc. Natl. Acad. Sci.* **114**, 13430 (2017).
- [12] B. Bleaney and M. R. Wells, Radiofrequency studies of tmvo_4 , *Proceedings of the Royal Society of London. Series A, Mathematical and Physical Sciences* **370**, 131 (1980).
- [13] G. J. Bowden, A review of the low temperature properties of the rare earth vanadates, *Australian Journal of Physics* **51**, 201 (1998).
- [14] G. A. Gehring and K. A. Gehring, Co-operative jahn-teller effects, *Reports on Progress in Physics* **38**, 1 (1975).
- [15] R. Feigenson, Flux growth of type RVO_4 rare-earth vanadate crystals, *Journal of the American Ceramic Society* **51**, 538 (1968).
- [16] S. Smith and B. Wanklyn, Flux growth of rare earth vanadates and phosphates, *Journal of Crystal Growth* **21**, 23 (1974).
- [17] B. Bleaney, J. Gregg, A. de Oliveira, and M. Wells, Nuclear electric quadrupole interaction in LnVO_4 , *Journal of Magnetism and Magnetic Materials* **31-34**, 745 (1983).
- [18] M. Lawson, B. T. Bush, T. Kissikov, Z. Brubaker, K. R. Shirer, J. R. Jeffries, S. Ran, I. Jeon, M. B. Maple, and N. J. Curro, Measurements of the NMR Knight shift tensor and nonlinear magnetization in URu_2Si_2 , *Phys. Rev. B* **97**, 075138 (2018).
- [19] D. M. Nisson, A. P. Dioguardi, P. Klavins, C. H. Lin, K. Shirer, A. C. Shockley, J. Crocker, and N. J. Curro, Nuclear magnetic resonance as a probe of electronic states of Bi_2Se_3 , *Phys. Rev. B* **87**, 195202 (2013).
- [20] A. Suter, M. Mali, J. Roos, and D. Brinkmann, Mixed magnetic and quadrupolar relaxation in the presence of a dominant static Zeeman Hamiltonian, *J. Phys.: Condens. Matter* **10**, 5977 (1998).
- [21] R. L. Melcher, E. Pytte, and B. A. Scott, Phonon instabilities in TmVO_4 , *Phys. Rev. Lett.* **31**, 307 (1973).
- [22] R. M. Fernandes, A. E. Böhrer, C. Meingast, and J. Schmalian, Scaling between magnetic and lattice fluctuations in iron pnictide superconductors, *Phys. Rev. Lett.* **111**, 137001 (2013).
- [23] K. M. Leung and D. L. Huber, Low-frequency dynamics in cooperative Jahn-Teller systems, *Physical Review B* **19**, 5483 (1979).
- [24] J. H. Page and S. R. P. Smith, Microwave ultrasonic attenuation above the Jahn-Teller phase transition in TmVO_4 , *Journal of Physics C: Solid State Physics* **16**, 309 (1983).
- [25] F. Borsa, M. Corti, and A. Rigamonti, Electronic spin-dynamics at a structural phase transition by cooperative Jahn-Teller effect: An Al^{27} NMR study in PrAlO_3 , *Journal of Applied Physics* **49**, 1383 (1978).
- [26] M. Corti, A. Rigamonti, and A. Magistris, ^{133}Cs quadrupole perturbed NMR study of jahn-teller phase transitions in CsCuCl_3 , *physica status solidi (b)* **108**, 29 (1981).
- [27] A. Rigamonti, NMR-NQR studies of structural phase transitions, *Advances in Physics* **33**, 115 (1984).
- [28] A. Smerald and N. Shannon, Angle-resolved NMR: Quantitative theory of ^{75}As T_1 relaxation rate in BaFe_2As_2 , *Phys. Rev. B* **84**, 184437 (2011).